

CondiQuant: Condition Number Based Low-Bit Quantization for Image Super-Resolution

Kai Liu^{1*}, Dehui Wang^{1*}, Zhiteng Li¹, Zheng Chen¹,
Yong Guo², Wenbo Li³, Linghe Kong^{1†}, Yulun Zhang^{1†}

¹Shanghai Jiao Tong University, ²South China University of Technology, ³Huawei Noah’s Ark Lab

Abstract

Low-bit model quantization for image super-resolution (SR) is a longstanding task that is renowned for its surprising compression and acceleration ability. However, accuracy degradation is inevitable when compressing the full-precision (FP) model to ultra-low bit widths (2 ~ 4 bits). Experimentally, we observe that the degradation of quantization is mainly attributed to the quantization of activation instead of model weights. In numerical analysis, the condition number of weights could measure how much the output value can change for a small change in the input argument, inherently reflecting the quantization error. Therefore, we propose **CondiQuant**, a **condition number based low-bit post-training quantization** for image super-resolution. Specifically, we formulate the quantization error as the condition number of weight metrics. By decoupling the representation ability and the quantization sensitivity, we design an efficient proximal gradient descent algorithm to iteratively minimize the condition number and maintain the output still. With comprehensive experiments, we demonstrate that CondiQuant outperforms existing state-of-the-art post-training quantization methods in accuracy without computation overhead and gains the theoretically optimal compression ratio in model parameters. Our code and model are released at <https://github.com/Kai-Liu001/CondiQuant>.

1. Introduction

Image super-resolution (SR) aims to restore the high-resolution (HR) images from the low-resolution counterparts. It is a foundational computer vision task in low-level vision and image processing, widely studied in medical imaging [11, 13, 15], surveillance [25, 36], remote sensing [1], and mobile phone photography [31]. Nonetheless, the existing edge devices’ notorious limited computation and memory ability hinder real-world deployment. Therefore, it is increasingly urgent to develop model compression and accel-

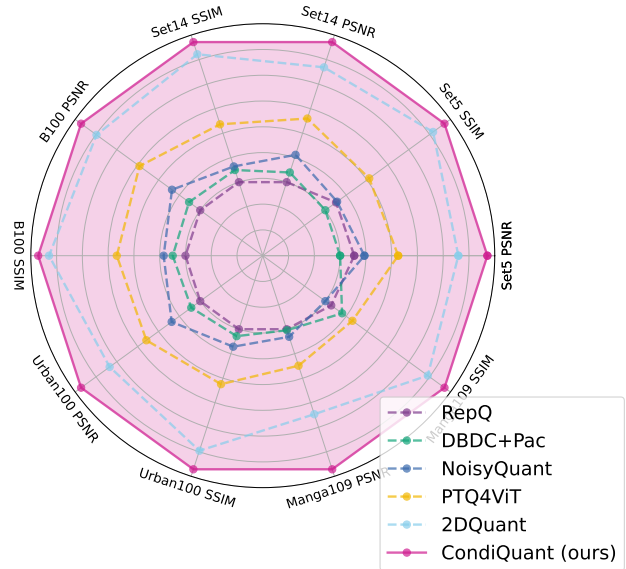


Figure 1. Comparison with SOTA PTQ methods on five benchmarks. Our CondiQuant gains consistently better performance. eration techniques for SR models to reduce the redundancy in both model parameters and inference computation.

Model quantization [5, 7, 14, 16] is a powerful compression technique that compresses the model from full-precision to low-bit representations. With quantization, the time-consuming floating-point operations are converted into efficient integer ones, making it an ideal candidate for model compression in resource-constrained edge devices. However, the conversion inevitably leads to severe performance degradation, especially when compressing to ultra-low bit width (*i.e.* 2 ~ 4 bits). The situation is more severe in vision transformers (ViTs) due to the deterioration of self-attention.

The two branches of quantization, aka quantization-aware training (QAT) and post-training quantization (PTQ), deal with the degradation in different ways. QAT, a firm adherent of backpropagation, concurrently optimizes the model weights and quantizers’ parameters via straight-through estimator (STE) [6]. Though inspiring results are obtained, the ineluctable demand for large datasets and long-time training discourages the deployment. Whereas, PTQ is much more

*Equal contribution.

†Corresponding authors: Yulun Zhang, yulun100@gmail.com; Linghe Kong, linghe.kong@sjtu.edu.cn

efficient. Most PTQ methods utilize efficient algorithms to calculate the quantizers’ parameters in a small calibration set. Given the complexity of both branches, PTQ is usually inferior to QAT and calls for advanced solutions.

To improve the inferior performance of PTQ, we observe two key experimental phenomena. The first observation is about the attribution of degradation.

Observation 1: *The degradation of quantization is mainly attributed to the quantization of activations.*

Therefore, we leverage condition number, a metric in numerical analysis, to reflect the changes caused by the quantization of activations. In detail, condition number could measure how much the output value can change given a disturbance in the input value, *i.e.* the quantization error of activation. Considering a small disturbance, the smaller the condition number is, the smaller the output varies. Thereafter, one way to reduce the quantization error is by minimizing the condition number of the weight matrix.

Inspired by MagR [35], we verify that their observation in LLMs also holds in SR models, which is

Observation 2: *The feature matrix X across all linear layers is approximately rank deficient.*

In a linear layer, the output Y can be expressed as matrix multiplication $Y = XW$, where W is the weight matrix and X is the feature matrix. When X is rank-deficient, there are infinite solutions for W that satisfy the equation. This desirable property allows a shift on the weight matrix to quantization friendliness while maintaining the output.

Based on the previous two observations, we focus on the impact of quantization of activation, establish its relationship with condition number, formulate the optimization problem, and derive proximal gradient descent to solve it efficiently. With the proposed CondiQuant, the restoration accuracy is improved evidently as shown in Fig. 1.

To sum up, our main contributions are fourfold:

1. We design CondiQuant, a novel PTQ method for image SR based on condition number. CondiQuant gains theoretically optimal compression and speedup ratios with currently minimum performance degradation.
2. We propose that the model’s sensitivity to quantization is related to the condition number of weights in the linear layers and could be hereby optimized efficiently.
3. We design an efficient algorithm based on proximal gradient descent to reduce the condition number of weight while approximately keeping the output still.
4. Comprehensive comparison experiments are conducted to show the state-of-the-art performance on efficiency and effectiveness of our proposed CondiQuant. Besides, extensive ablation studies are conducted to prove the robustness and efficacy of our proposed CondiQuant.

2. Related Work

Image Super-Resolution. The trailblazing research on image super-resolution with deep neural network is SR-CNN [8], which utilizes convolution layers to replace conventional methods in SR. Since then, dazzling network architectures [3, 4, 19, 37] are designed to achieve more stirring image restoration accuracy. RDN [38] designs dense skip connection and global residual to utilize abundant local and global features. With the advance of vision transformer, SwinIR [18] uses window-attention to fully make use of global information. As reconstruction accuracy increases, researchers focus more on model parameters and operations. Generally, the ViT-based SR networks are much smaller and faster than pure CNNs. However, even the advanced SR networks like SwinIR, current SR models are still too large to be deployed on resource-constrained edge devices. Therefore, research on quantization on ViT-based networks is urgently needed to make SR possible on mobile devices.

Post-Training Quantization. PTQ is famous for its fast speed and low cost during quantization. Recently, excellent PTQ methods have been proposed to advance its performance and efficiency. As a PTQ method specifically for ViT, PTQ4ViT [33] proposed twin uniform quantization to reduce quantization error on the output of softmax and GELU. RepQ [17] decouples the quantization and inference processes and ensures both accurate quantization and efficient inference. NoisyQuant [21] surprisingly finds that adding a fixed Uniform noisy bias to the values being quantized can significantly reduce the quantization error. However, most of the above PTQ methods are only for Transformer blocks and the generalization ability on SR tasks is relatively low. Whereas, 2DQuant [20] searches the clipping bounds in different ways on different distributions and is currently the best PTQ method on the SR task. However, most of the above methods only concentrate on the quantization process and ignore adjustments in the weights.

Condition Number. The concept of the condition number originated and developed in numerical analysis [28, 29]. It measures how much the output value of the system or function can change for a small change in the input. A matrix with a high condition number is said to be ill-conditioned and leads to huge output changes given a small disturbance in input. It also plays an important role in machine learning (ML). Freund proposed optimization algorithms generally converge faster when the condition number is low [9]. In causal inference, it is used to evaluate the numerical stability of causal effect estimation [10]. Additionally, the condition number is leveraged to enhance the numerical stability of regression models by fine-tuning hidden layer parameters [32]. In this work, we innovatively leverage the condition number into quantization to measure the quantization sensitivity. We formulate the optimization of quantization error via condition number and propose CondiQuant to solve it efficiently.

	Y	Y + XδW	Y + δXW	Y + δXδW
PSNR	32.2543	32.0117	31.3304	32.2519
SSIM	0.9293	0.9270	0.9221	0.9293

Table 1. Attribution of quantization loss. Y denotes the FP model and the rest denotes performing quantization on W , X , and both.

3. Method

3.1. Preliminaries

Given an SR network, we use upper and lower clipping bounds to quantize weights and activations [20]. Usually, we leverage the fake quantization to simulate the quantization process with no simulation error. The fake-quantize process, *i.e.* quantization-dequantization, can be written as:

$$x_c = \text{Clip}(x, l, u), x_r = \mathbf{R}(s(x_c - l)), x_q = sx_r + l, \quad (1)$$

where x denotes weight w or activation a being quantized and $s = (2^N - 1)/(u - l)$ is the quantization ratio. l and u denote the lower bound and upper bound for clipping, respectively. $\text{Clip}(x, l, u) = \min(\max(x, l), u)$ constrains the input to be between l and u , and $\mathbf{R}(\cdot)$ rounds the input to its nearest integer. With the above process, the continuous values are dispersed into discrete candidates.

3.2. Analysis

To analyze the loss attribution in quantization, we first rewrite the linear layer with quantization as follows:

$$\begin{aligned} \hat{Y} &:= \hat{X}\hat{W} = (X + \delta X)(W + \delta W) \\ &= XW + X\delta W + \delta XW + \delta X\delta W, \end{aligned} \quad (2)$$

where \hat{X} denotes the quantized value and δX denotes the quantization error of X . The second-order term $\delta X\delta W$ can be ignored due to its tiny impact on performance. Thus Eq. (2) can be rewritten as:

$$\hat{Y} \approx XW + X\delta W + \delta XW = Y + X\delta W + \delta XW. \quad (3)$$

Additionally, we observe that the negative influence of $X\delta W$ and $\delta X\delta W$ is much smaller than δXW , shown in Table 1. This result can be explained for two reasons. First, the activation varies with different inputs while the weight is fixed. Therefore, the average value of the absolute value of the δX elements is much greater than that of δW . Second, the W is sensitive to minor changes, *i.e.* δX . Hence, we only concentrate on δXW and ignore $X\delta W$ in the following discussion. So we can further approximate the loss:

$$\hat{Y} \approx XW + \delta XW, \quad \delta Y \approx \delta XW. \quad (4)$$

Eq. (4) indicates that the degradation of model performance can be divided into two components: (1) the magnitude of activation quantization error and the sensitivity of the weight to disturbance. To minimize the approximate loss, a naive solution is to reduce the Frobenius norm of δX *i.e.* $\|\delta X\|_F$. However, it is unpractical as δX varies with different inputs, and rounding-off errors are impossible to reduce especially with ultra-low bits. Therefore, we focus on the model’s sensitivity to quantization, related to condition number.

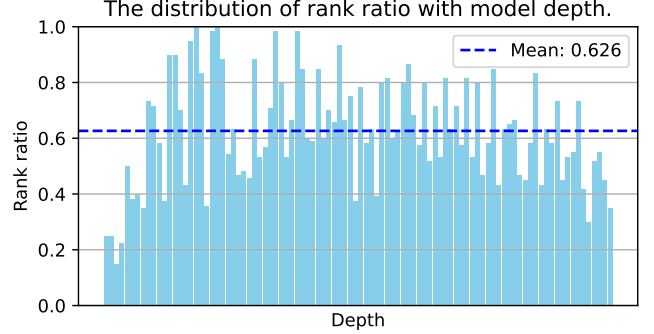


Figure 2. Distribution of activation ranks along the ($\times 2$) model depth. Most activations are severely rank deficient.

3.3. CondiQuant

We begin with the observation of rank deficiency of the feature matrix. Then we derive the optimization objective and illustrate the methodology to arrive at the solution.

Rank Deficiency. We visualize the rank ratio in Fig. 2. Most of the layers are rank deficient and only two layers are full rank. The mean value of the rank ratio is 0.626. In the linear layer, the process is matrix multiplication, *i.e.* $Y = XW$. If W is rank deficient, there exist infinite W' that satisfies $XW = XW'$. Hence, this result serves as a theory foundation to select W' to minimize δXW .

Formulation. In this section, we formulate the relationship between model sensitivity and condition number. We begin with the inequality of $\|\delta Y\|_2$ and $\|Y\|_2$:

$$\|\delta Y\|_2 = \|\delta XW\|_2 \leq \|\delta X\|_2 \|W\|_2, \quad (5)$$

$$\|Y\|_2 = \|XW\|_2 \geq \|X\|_2 \sigma_{\min}(W), \quad (6)$$

where $\|\cdot\|_2$ is the bi-norm of the matrix, and $\sigma_{\min}(\cdot)$ denotes the minimum singular value. Combining Eq. (5) and Eq. (6), we can establish the relationship between quantization loss and condition number, which can be written as:

$$\frac{\|\delta Y\|_2}{\|Y\|_2} \leq \frac{\|\delta X\|_2 \|W\|_2}{\|X\|_2 \sigma_{\min}(W)} = \kappa(W) \frac{\|\delta X\|_2}{\|X\|_2}, \quad (7)$$

where $\kappa(W)$ denotes the condition number of W . This formula shows that under the same rounding-off error, the impact of quantization is greater with larger $\kappa(W)$. Detailed derivation can be found in the supplementary materials. Therefore, we minimize the condition number of W and maintain the output. The objective can be written as:

$$\min_W \kappa(W) = \frac{\sigma_{\max}(W)}{\sigma_{\min}(W)}, \text{ s.t. } \|XW - X\hat{W}\|_F \leq \epsilon, \quad (8)$$

where ϵ is a small positive number that limits the magnitude of the loss. However, it is a non-convex and non-smooth optimization when minimizing the condition number directly. To address this, we construct a proxy objective function to enable optimization and propose the proximal gradient method as an effective approach for solving it.

Proxy objective function. To minimize the condition number, our strategy is to compact the distribution of all singular values as densely as possible. Specifically, we design a regu-

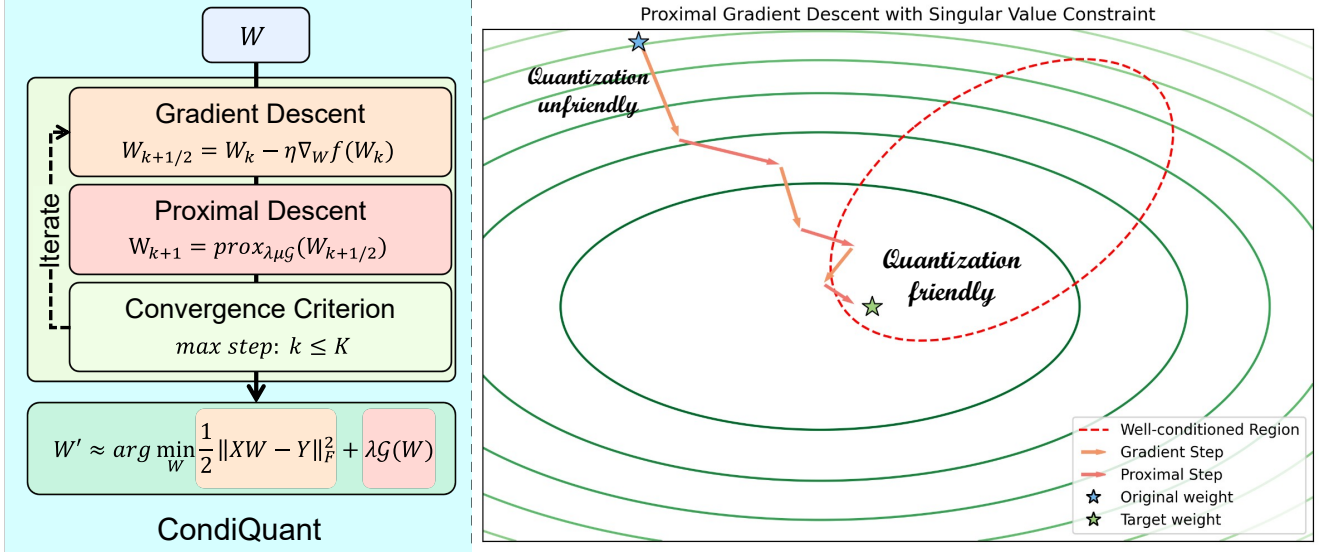


Figure 3. Overview of our proposed CondiQuant which employs iterative optimization to minimize the condition number of weight matrix while maintaining the output still. The gradient descent step updates the weight matrix with gradients to ensure the output is close to the original. The proximal descent step minimizes the condition number with the proximal operator. The above two steps are conducted iteratively before reaching the convergence criterion, *i.e.* the max iteration step. We illustrate the effect of both steps. With CondiQuant, the weight matrix is converted into a quantization-friendly and well-conditioned one while the output is close to the original.

larization term to minimize the deviation of singular values:

$$\min_W \frac{1}{2} \|XW - Y\|_F^2 + \lambda \cdot \mathcal{G}(W), \quad (9)$$

where $\mathcal{G}(\cdot)$ is a regularization term used to compact the singular value distribution and λ is the regularization strength parameter. There are several forms of $\mathcal{G}(W)$ to compact the singular values' distribution. Considering efficiency and effect, we choose the following form:

$$\mathcal{G}(W) := \sum_{i=1}^r (\sigma_i(W) - t)^2, \quad (10)$$

where $r = \text{rank}(W)$ represents the number of singular values and t is a value between $\sigma_{\min}(W)$ and $\sigma_{\max}(W)$. The median or the mean of the singular values are possible candidates for t and we choose the mean value form in CondiQuant. With this form, we could provide a closed solution to minimize $\mathcal{G}(W)$ in the following section.

Proximal Operator for $\mathcal{G}(W)$. We utilize the proximal operator to minimize the $\mathcal{G}(W)$ part. We define the proximal operator of function $\mathcal{G}(W)$ as follows:

$$\text{prox}_{\lambda \mu \mathcal{G}}(W) := \arg \min_Z \left\{ \frac{1}{2} \|Z - W\|_F^2 + \lambda \mu \mathcal{G}(Z) \right\}, \quad (11)$$

where μ is a hyper-parameter to balance the optimization. The target of Eq. (11) is to minimize $\mathcal{G}(Z)$ and keep Z close to W . To solve this problem, we perform singular value decomposition (SVD) on W to extract the singular values:

$$W = U \Sigma_W V^T, \quad (12)$$

where U and V are orthogonal matrices and $\Sigma_W = \text{diag}(\sigma_i(V))$ is the diagonal matrix of singular values. The problem could be reduced to optimize each singular value

$\sigma_i(W)$ independently and can be written as:

$$\sigma_i^*(W) := \arg \min_{\sigma_i^*} \left\{ \frac{1}{2} (\sigma_i^* - \sigma_i(W))^2 + \lambda \mu (\sigma_i^* - t)^2 \right\}. \quad (13)$$

We notice that Eq. (13) is a quadratic minimization problem and a closed solution could be derived. Specifically, after taking the derivative and setting it to zero, we have:

$$\sigma_i^*(W) = \frac{\sigma_i(W) + 2\lambda \mu t}{1 + 2\lambda \mu}. \quad (14)$$

Using the updated singular values $\sigma_i^*(W)$, we reconstruct the matrix with lower condition number:

$$W^* = U \Sigma_{W^*} V^T, \quad \Sigma_{W^*} = \text{diag}(\sigma_i^*(W)). \quad (15)$$

To conclude, with the proximal operator, we could update W to W^* to minimize $\mathcal{G}(W)$. Hereby, the condition number of W is reduced and the output is kept still.

Proximal Gradient Descent. As discussed previously, the optimization problem contains both smooth and non-smooth components. More specifically, $\frac{1}{2} \|XW - Y\|_F^2$ is a convex and differentiable function, while $\mathcal{G}(W)$ is a convex but non-differentiable function. With the proximal operator, we design the proximal gradient descent method to solve two components iteratively. The iterative steps are as follows:

Step1. Gradient Descent. Compute the updated value of the smooth part $\frac{1}{2} \|XW - Y\|_F^2$ with the gradient descent:

$$W_{k+\frac{1}{2}} = W_k - \eta \nabla_W \frac{1}{2} \|XW - Y\|_F^2 \Big|_{W=W_k}, \quad (16)$$

where $\eta > 0$ is the step size, and ∇_W is the gradient of $\frac{1}{2} \|XW - Y\|_F^2$ at W_k . With this step, we ensure the output is as consistent as possible with the original value.

η	10^{-1}	10^{-2}	10^{-3}	10^{-4}	t	Mean value	Median value	$(\sigma_{max} + \sigma_{min})/2$
PSNR \uparrow	37.13	37.15	37.15	37.08	PSNR \uparrow	37.15	37.12	37.11
SSIM \uparrow	0.9568	0.9568	0.9567	0.9564	SSIM \uparrow	0.9567	0.9566	0.9567

(a) Ablation study on learning rate η .

λ	0.001	0.002	0.003	0.004	0.005	0.010		2DQuant	w/o CondiQuant	w/ CondiQuant
PSNR \uparrow	37.13	37.12	37.15	37.13	37.10	37.08	PSNR \uparrow	36.00	37.08	37.15
SSIM \uparrow	0.9567	0.9566	0.9567	0.9567	0.9566	0.9565	SSIM \uparrow	0.9497	0.9557	0.9567

(c) Ablation study on Regularization coefficient λ .

(b) Ablation study on target value t .

(d) Ablation study on CondiQuant.

Table 2. Ablation studies of CondiQuant on Set5 ($\times 2$, 2 bits). The selections of hyper-parameters and the effect of CondiQuant are detailedly evaluated. The results demonstrate that CondiQuant is robust and can improve performance significantly.

Step2. Proximal Step. Apply the proximal operator to the non-smooth part $\mathcal{G}(W)$ with Eq. (12), Eq. (14) and Eq. (15) to minimize the condition number:

$$\tilde{W}_k = \text{prox}_{\lambda\mu\mathcal{G}}(W_{k+\frac{1}{2}}) = U\Sigma_{W^*}V^T.$$

Step3. Repeat. Iterate the above two steps until reaching the convergence criterion, *i.e.* $k \geq K$. k is the iteration step while K is the total step of iteration. We select a desired K such that the difference between consecutive iterates is sufficiently small while the iteration is not too long.

We illustrate our proposed CondiQuant in Fig. 3. With the proposed CondiQuant, we convert the weight metric from the quantization-unfriendly position into a friendly position. Besides, both gradient descent and proximal descent steps are calculation efficient and the cost is inexpensive. Moreover, we introduce no additional module. Therefore, no computation and storage overhead is caused during the inference stage and we obtain the theoretic optimal compression and speedup ratio in post-training quantization. After the conversion, we leverage the previous work’s scheme [20] to perform quantization and calibration with modification and the details are described in the supplementary materials.

4. Experiments

To exhibit the outstanding performance of our proposed CondiQuant, comparisons with SOTA methods are also provided in both quantitative and qualitative forms. Extensive ablation studies are conducted to show the robustness and effectiveness of our elaborate designs.

4.1. Experimental Settings

Data and Evaluation. We employ DF2K [19, 26] as the calibration set, which combines DIV2K [26] and Flickr2K [19]. During calibration, we only use low-resolution ones and the FP model. Thereafter, CondiQuant is tested on five commonly used benchmarks in the SR field, including Set5 [2], Set14 [34], B100 [22], Urban100 [12], and Manga109 [23]. The evaluation metrics include PSNR and SSIM [30], which are calculated on the Y channel of the YCbCr space.

Implementation Details. The backbone of CondiQuant is SwinIR-light [18], a small and efficient ViT for image restoration. The scale factors include $\times 2$, $\times 3$, and $\times 4$, and bit-width includes 2, 3, and 4 bits. During condition number

optimization, the calibration set size is 100 images, randomly selected from DF2K and cropped to $3 \times 64 \times 64$. We set step size $\eta = 10^{-2}$, regularization coefficient $\lambda = 0.003$, $\mu = 1$, and max iteration $K = 50$. The target value t is the mean value of singular values. Our code is written with PyTorch [24] and runs on an NVIDIA A800-80GB GPU.

4.2. Ablation Study

In this section, we conduct four ablation studies on Set5 ($\times 2$) with 2 bits to evaluate the robustness of our design.

Learning Rate η . In CondiQuant, η decides the step size of the gradient descent step. We evaluate η from 10^{-4} to 10^{-1} . As shown in Tab. 2a, the impact of η is minor in the evaluation range. We attribute this minor impact to the rank deficiency across the network and the design of proximal descent. Rank deficiency allows multiple candidates for W while the SVD reconstruction also guarantees the output remains the same. Therefore, the difference between $W_{k+\frac{1}{2}}$ and \tilde{W}_k is small enough. However, the gradient step is not unnecessary as it ensures the output won’t change much.

Selection of t . As discussed in Sec. 3.3, there are several ways to select the target value t in $\mathcal{G}(W)$, including the mean value and median value of all singular values and $(\sigma_{min} + \sigma_{max})/2$. We try these variants and the result is shown in Tab. 2b. The stable performance with different variants indicates that so long as the singular values are compacted, the performance could be therefore improved. So we choose the mean value of singular values to assign t .

Regularization Coefficient λ . As shown in Tab. 2c, we test different λ from 0.001 to 0.01. The optimal results could be obtained when λ is set to 0.003 while other values also provide well enough PSNR and SSIM.

CondiQuant. As shown in Tab. 2d, the existence of CondiQuant is impactful. 2DQuant provides relatively inferior results while our modification improves the performance significantly. Besides, CondiQuant could ease the quantization difficulty and further improve the performance. Moreover, CondiQuant only takes less than 19.0 seconds to perform and the computation overhead is minor. Hence, CondiQuant could serve as an efficient pre-processing technique before model quantization, especially with ultra-low bit width.

Table 3. Quantitative comparison with SOTA methods. The first and second highest methods are marked with **red** and **blue** respectively. Our proposed CondiQuant remarkably outperforms **all** other methods in **all** settings on **all** benchmarks.

Method	Bit	Set5 ($\times 2$)		Set14 ($\times 2$)		B100 ($\times 2$)		Urban100 ($\times 2$)		Manga109 ($\times 2$)	
		PSNR \uparrow	SSIM \uparrow	PSNR \uparrow	SSIM \uparrow	PSNR \uparrow	SSIM \uparrow	PSNR \uparrow	SSIM \uparrow	PSNR \uparrow	SSIM \uparrow
SwinIR-light [18]	32	38.15	0.9611	33.86	0.9206	32.31	0.9012	32.76	0.9340	39.11	0.9781
Bicubic	32	32.25	0.9118	29.25	0.8406	28.68	0.8104	25.96	0.8088	29.17	0.9128
DBDC+Pac [27]	4	37.18	0.9550	32.86	0.9106	31.56	0.8908	30.66	0.9110	36.76	0.9692
PTQ4ViT [33]	4	37.43	0.9571	33.19	0.9139	31.84	0.8950	31.54	0.9212	37.59	0.9735
RepQ [17]	4	37.89	0.9600	33.47	0.9174	32.08	0.8975	31.98	0.9269	38.37	0.9763
NoisyQuant [21]	4	37.50	0.9570	33.06	0.9101	31.73	0.8936	31.31	0.9181	37.47	0.9723
2DQuant [20]	4	37.87	0.9594	33.41	0.9161	32.02	0.8971	31.84	0.9251	38.31	0.9761
CondiQuant (ours)	4	38.03	0.9605	33.50	0.9180	32.16	0.8993	32.03	0.9282	38.57	0.9769
DBDC+Pac [27]	3	35.07	0.9350	31.52	0.8873	30.47	0.8665	28.44	0.8709	34.01	0.9487
PTQ4ViT [33]	3	36.49	0.9510	32.49	0.9045	31.27	0.8854	30.16	0.9027	36.41	0.9673
RepQ [17]	3	35.06	0.9325	31.29	0.8719	30.04	0.8512	29.17	0.8726	34.89	0.9518
NoisyQuant [21]	3	35.32	0.9334	31.88	0.8911	30.73	0.8710	29.28	0.8835	35.30	0.9537
2DQuant [20]	3	37.32	0.9567	32.85	0.9106	31.60	0.8911	30.45	0.9086	37.24	0.9722
CondiQuant (ours)	3	37.77	0.9594	33.21	0.9151	31.94	0.8966	31.18	0.9197	38.01	0.9755
DBDC+Pac [27]	2	34.55	0.9386	31.12	0.8912	30.27	0.8706	27.63	0.8649	32.15	0.9467
PTQ4ViT [33]	2	33.25	0.8923	30.22	0.8402	29.21	0.8066	27.31	0.8111	32.75	0.9093
RepQ [17]	2	31.65	0.8327	29.19	0.7789	28.27	0.7414	26.56	0.7455	30.46	0.8268
NoisyQuant [21]	2	30.13	0.7620	28.80	0.7556	28.26	0.7421	26.68	0.7627	30.40	0.8204
2DQuant [20]	2	36.00	0.9497	31.98	0.9012	30.91	0.8810	28.62	0.8819	34.40	0.9602
CondiQuant (ours)	2	37.15	0.9567	32.74	0.9103	31.55	0.8912	29.96	0.9047	36.63	0.9713
Method	Bit	Set5 ($\times 3$)		Set14 ($\times 3$)		B100 ($\times 3$)		Urban100 ($\times 3$)		Manga109 ($\times 3$)	
SwinIR-light [18]	32	34.63	0.9290	30.54	0.8464	29.20	0.8082	28.66	0.8624	33.99	0.9478
Bicubic	32	29.54	0.8516	27.04	0.7551	26.78	0.7187	24.00	0.7144	26.16	0.8384
DBDC+Pac [27]	4	33.42	0.9143	29.69	0.8261	28.51	0.7869	27.05	0.8217	31.89	0.9274
PTQ4ViT [33]	4	33.77	0.9201	29.75	0.8272	28.62	0.7942	27.43	0.8361	32.50	0.9360
RepQ [17]	4	34.08	0.9232	30.04	0.8345	28.88	0.8013	27.87	0.8462	32.98	0.9401
NoisyQuant [21]	4	33.13	0.9122	29.06	0.8093	27.93	0.7754	26.66	0.8143	31.94	0.9293
2DQuant [20]	4	34.06	0.9231	30.12	0.8374	28.89	0.7988	27.69	0.8405	32.88	0.9389
CondiQuant (ours)	4	34.32	0.9260	30.29	0.8417	29.05	0.8039	28.05	0.8506	33.23	0.9431
DBDC+Pac [27]	3	30.91	0.8445	28.02	0.7538	26.99	0.6937	25.10	0.7122	28.84	0.8403
PTQ4ViT [33]	3	32.75	0.9028	29.14	0.8113	28.06	0.7712	26.43	0.8014	31.20	0.9131
RepQ [17]	3	31.04	0.8548	28.04	0.7572	26.83	0.7019	25.56	0.7493	30.16	0.8904
NoisyQuant [21]	3	30.78	0.8511	27.94	0.7624	26.98	0.7153	25.43	0.7481	29.64	0.8792
2DQuant [20]	3	33.24	0.9135	29.56	0.8255	28.50	0.7873	26.65	0.8116	31.46	0.9235
CondiQuant (ours)	3	33.92	0.9224	30.02	0.8367	28.84	0.7986	27.37	0.8356	32.48	0.9367
DBDC+Pac [27]	2	29.96	0.8254	27.53	0.7507	27.05	0.7136	24.57	0.7117	27.23	0.8213
PTQ4ViT [33]	2	29.96	0.7901	27.36	0.7030	26.74	0.6590	24.56	0.6460	27.37	0.7390
RepQ [17]	2	27.32	0.6478	25.63	0.5918	25.44	0.5652	23.42	0.5582	24.51	0.5721
NoisyQuant [21]	2	27.53	0.6641	25.77	0.5952	25.37	0.5613	23.59	0.5739	26.03	0.6632
2DQuant [20]	2	31.62	0.8887	28.54	0.8038	27.85	0.7679	25.30	0.7685	28.46	0.8814
CondiQuant (ours)	2	33.00	0.9130	29.44	0.8253	28.45	0.7882	26.36	0.8080	30.88	0.9203
Method	Bit	Set5 ($\times 4$)		Set14 ($\times 4$)		B100 ($\times 4$)		Urban100 ($\times 4$)		Manga109 ($\times 4$)	
SwinIR-light [18]	32	32.45	0.8976	28.77	0.7858	27.69	0.7406	26.48	0.7980	30.92	0.9150
Bicubic	32	27.56	0.7896	25.51	0.6820	25.54	0.6466	22.68	0.6352	24.19	0.7670
DBDC+Pac [27]	4	30.74	0.8609	27.66	0.7526	26.97	0.7104	24.94	0.7369	28.52	0.8697
PTQ4ViT [33]	4	31.49	0.8831	28.04	0.7680	27.20	0.7240	25.53	0.7660	29.52	0.8940
RepQ [17]	4	31.77	0.8880	28.32	0.7750	27.40	0.7310	25.83	0.7780	29.88	0.9010
NoisyQuant [21]	4	31.09	0.8751	27.75	0.7591	26.91	0.7151	25.07	0.7500	28.96	0.8820
2DQuant [20]	4	31.77	0.8867	28.30	0.7733	27.37	0.7278	25.71	0.7712	29.71	0.8972
CondiQuant (ours)	4	32.09	0.8923	28.50	0.7792	27.52	0.7345	25.97	0.7831	30.16	0.9054
DBDC+Pac [27]	3	27.91	0.7250	25.86	0.6451	25.65	0.6239	23.45	0.6249	26.03	0.7321
PTQ4ViT [33]	3	29.77	0.8337	27.00	0.7248	26.21	0.6735	24.22	0.6983	27.94	0.8479
RepQ [17]	3	27.52	0.7419	24.84	0.5996	23.99	0.5351	22.42	0.5739	26.58	0.7838
NoisyQuant [21]	3	28.90	0.7972	26.50	0.6970	26.16	0.6628	23.86	0.6667	27.17	0.8116
2DQuant [20]	3	30.90	0.8704	27.75	0.7571	26.99	0.7126	24.85	0.7355	28.21	0.8683
CondiQuant (ours)	3	31.62	0.8855	28.20	0.7715	27.31	0.7269	25.39	0.7624	29.29	0.8915
DBDC+Pac [27]	2	25.01	0.5554	23.82	0.4995	23.64	0.4544	21.84	0.4631	23.63	0.5854
PTQ4ViT [33]	2	27.23	0.6702	25.38	0.5914	25.15	0.5621	22.94	0.5587	24.66	0.6132
RepQ [17]	2	25.55	0.5834	23.54	0.4751	23.30	0.4298	21.62	0.4493	23.60	0.5561
NoisyQuant [21]	2	25.94	0.5862	24.33	0.5067	24.16	0.4718	22.32	0.4841	23.82	0.5403
2DQuant [20]	2	29.53	0.8372	26.86	0.7322	26.46	0.6927	23.84	0.6912	26.07	0.8163
CondiQuant (ours)	2	30.64	0.8671	27.59	0.7567	26.93	0.7136	24.54	0.7282	27.67	0.8613

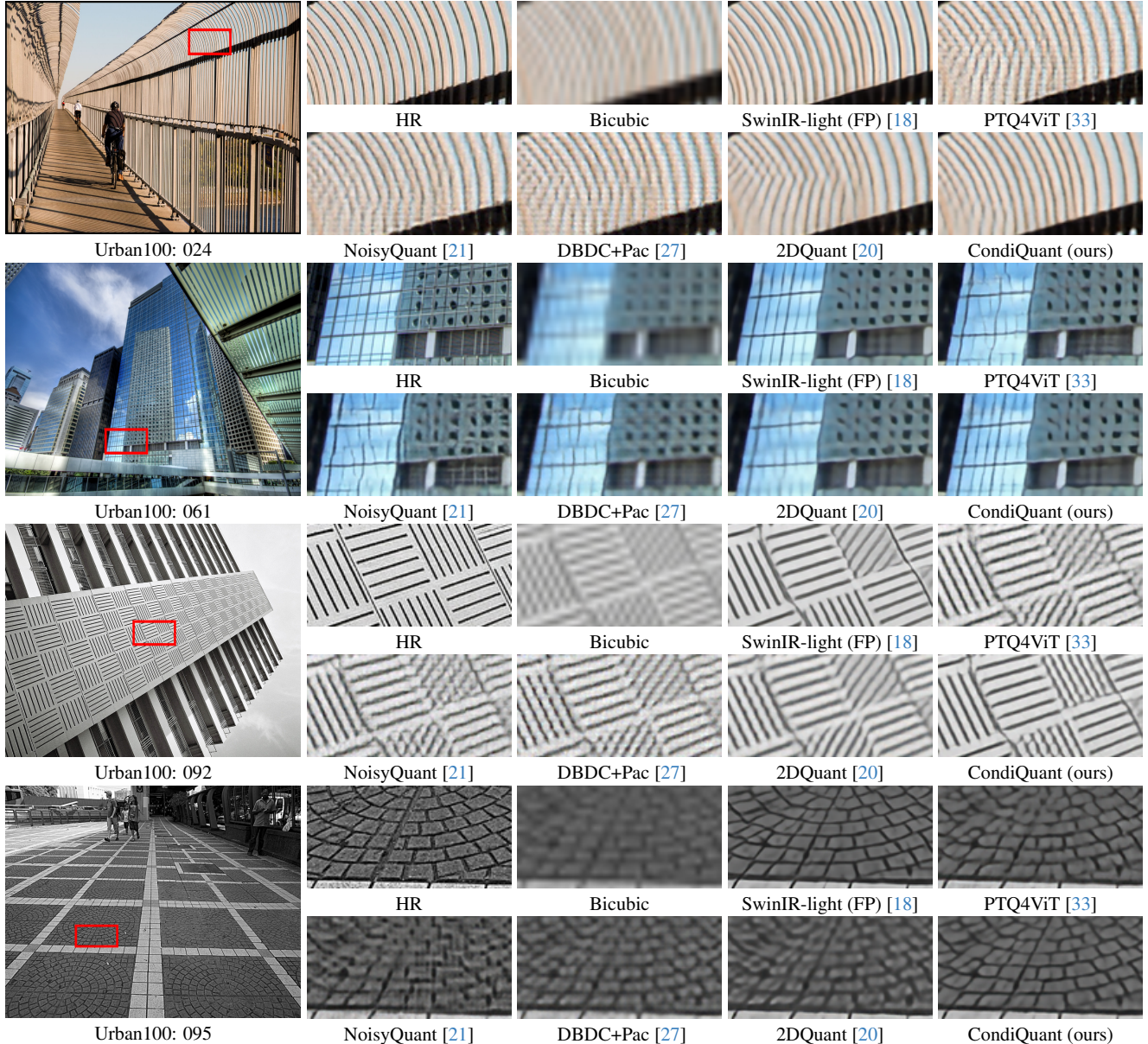


Figure 4. Visual comparison for image SR. We compare our proposed CondiQuant with current competitive quantization methods and the full-precision (FP) model. The visual results illustrate that CondiQuant gains sharper edges and reasonable textures.

4.3. Comparison with State-of-the-Art Methods

We adopt two kinds of SOTA PTQ methods for comparison. The first kind is PTQ methods specifically for SR, including DBDC+Pac [27], 2DQuant [20]. The second kind includes PTQ4ViT [33], RepQ [17], and NoisyQuant [21], which are designed for general vision transformers.

Quantitative Results. Table 3 shows the comprehensive results comparing with edge PTQ methods with $2 \sim 4$ bits and $2 \sim 4$ scale factors on five common SR benchmarks. With two universally accepted metrics, our proposed CondiQuant outperforms all other methods on all benchmarks regardless of bit-width, and scale factor. Specifically, CondiQuant has a huge improvement of 1.11 dB and 1.60 dB on $\times 4$, 2-bit

on Set5 and Manga109 datasets respectively. Besides, the average difference between $\times 2$, 4 bits CondiQuant, and the full-precision model is 0.38 dB. This means the quantization degradation when compressing to only 4 bits is minimal, and small enough for real-world deployment on edge devices.

With condition number optimization, the model’s sensitivity to the quantization error is reduced. Thereafter, the weight matrix is efficiently converted into a more quantization-friendly representation. Furthermore, the quantized model enjoys significant improvement during the following calibration and distillation stage. Besides, the oscillation during distillation is reduced, and detailed supporting information is in supplemental material.

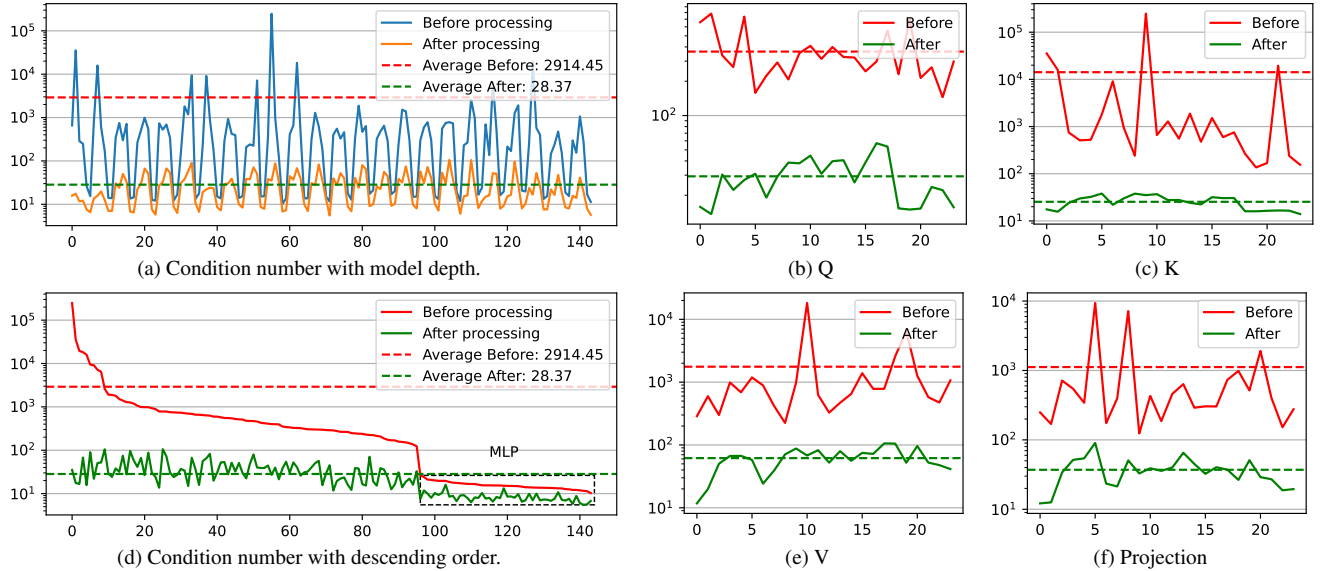


Figure 5. Condition number before and after CondiQuant on $\times 2$ model. Before CondiQuant, the distribution of condition numbers is extremely high, with an average of nearly 3k. After CondiQuant, the average value of condition numbers is significantly reduced to 28.37.

Visual Results. We present the visual comparison results of $\times 4$ in Fig. 4. The competing methods are struggling to recover inerratic textures and often generate artifacts. On the contrary, with our proposed CondiQuant, the quantized model could reconstruct HR with rich details and reasonable structures. In 024 and 061, the direction of the texture is distorted, and jagged edges are generated with Bicubic. Given the misleading input, other methods can not provide robust restoration like the FP model. However, our proposed CondiQuant can still guarantee fidelity to the greatest extent.

Even more, in 092, the FP model can not provide results with accurate direction on the wall while CondiQuant can correct the error and provide sharp contents. This is because the FP model suffers from over-fitting and CondiQuant could ease this phenomenon. Besides, in 095, the competing methods recover bricks with vague texture while CondiQuant keeps aligned with the FP model. In conclusion, compared to other methods, CondiQuant achieves the minimum information loss after low bit quantization and restores images with high-fidelity, rich details, and shaper edges.

4.4. Condition Number Analysis

The excellent results are closely related to the decrease in condition number. Therefore, we visualize the condition number shifts in Fig. 5 on the SR model with the scale factor of 2. Figures 5a and 5d show the condition number of all layers (including Q, K, V, projection, FC1, and FC2) with different sequences. Fig. 5a is about model depth and Fig. 5d sorts the condition number before CondiQuant with descending order. The other four figures show different layers with model depth as the X-axis.

Overall, the average condition number is hugely reduced from nearly 3k to merely 28.37. This evident decrease shows

the effectiveness of the proximal descent step in CondiQuant. To be specific, a regular pattern is observed with model depth. The condition numbers of the FC1 and FC2 in the MLP layer are distinctly smaller than those of other layers, and their influence is also minor. Hence, considering efficiency, we do not perform CondiQuant on FC1 and FC2. The condition number of the K matrix in self-attention is usually extremely great. This is also consistent with the claim that the quantization degradation of ViT is mainly attributed to self-attention. Moreover, the distribution of the condition number after CondiQuant is greater in the middle and smaller in both ends. This indicates that the beginning and end modules are more important and insensitive in image restoration. To conclude, our proposed CondiQuant significantly reduces the condition number with high efficiency.

5. Conclusion

In this paper, we propose CondiQuant, a condition number based post-training quantization method for image super-resolution. We analyze that the degradation of quantization is attributed to the quantization of activation and build its relationship with condition number. Thereafter, we formulate the optimization problem to minimize the condition number while maintaining the output as it is. To optimize, we design the gradient descent step to keep the output still and the proximal descent step to reduce the condition number. Both steps are calculation efficient and the entire iteration process takes only 19.0 seconds. As there’s no additional module, we reach the theoretically optimal compression and speedup ratio. Specifically, when quantized to 2 bits, the compression ratio is $3.60\times$ and the speedup ratio is $5.08\times$. The comparison experiments demonstrate the excellent performance of CondiQuant while the ablation studies present its robustness.

References

- [1] Wele Gedara Chaminda Bandara and Vishal M. Patel. Hypertransformer: A textural and spectral feature fusion transformer for pansharpening. In *CVPR*, 2022. 1
- [2] Marco Bevilacqua, Aline Roumy, Christine Guillemot, and Marie Line Alberi-Morel. Low-complexity single-image super-resolution based on nonnegative neighbor embedding. In *BMVC*, 2012. 5
- [3] Zheng Chen, Yulun Zhang, Jinjin Gu, Yongbing Zhang, Linghe Kong, and Xin Yuan. Cross aggregation transformer for image restoration. In *NeurIPS*, 2022. 2
- [4] Zheng Chen, Yulun Zhang, Jinjin Gu, Linghe Kong, Xiaokang Yang, and Fisher Yu. Dual aggregation transformer for image super-resolution. In *CVPR*, 2023. 2
- [5] Yoni Choukroun, Eli Kravchik, Fan Yang, and Pavel Kisilev. Low-bit quantization of neural networks for efficient inference. In *ICCVW*, 2019. 1
- [6] Matthieu Courbariaux, Itay Hubara, Daniel Soudry, Ran El-Yaniv, and Yoshua Bengio. Binarized neural networks: Training deep neural networks with weights and activations constrained to+ 1 or-1. *arXiv preprint arXiv:1602.02830*, 2016. 1
- [7] Yifu Ding, Haotong Qin, Qinghua Yan, Zhenhua Chai, Junjie Liu, Xiaolin Wei, and Xianglong Liu. Towards accurate post-training quantization for vision transformer. In *ACM MM*, 2022. 1
- [8] Chao Dong, Chen Change Loy, Kaiming He, and Xiaoou Tang. Image super-resolution using deep convolutional networks. *TPAMI*, 2016. 2
- [9] Robert M. Freund, Paul Grigas, and Rahul Mazumder. Condition number analysis of logistic regression, and its implications for standard first-order solution methods. *arXiv preprint arXiv:1810.08727*, 2018. 2
- [10] Spencer L. Gordon, Vinayak M. Kumar, Leonard J. Schulman, and Piyush Srivastava. Condition number bounds for causal inference. *PMLR*, 2021. 2
- [11] Hayit Greenspan. Super-resolution in medical imaging. *The Computer Journal*, 2008. 1
- [12] Jia-Bin Huang, Abhishek Singh, and Narendra Ahuja. Single image super-resolution from transformed self-exemplars. In *CVPR*, 2015. 5
- [13] Yawen Huang, Ling Shao, and Alejandro F Frangi. Simultaneous super-resolution and cross-modality synthesis of 3d medical images using weakly-supervised joint convolutional sparse coding. In *CVPR*, 2017. 1
- [14] Itay Hubara, Yury Nahshan, Yair Hanani, Ron Banner, and Daniel Soudry. Accurate post training quantization with small calibration sets. In *ICML*, 2021. 1
- [15] Jithin Saji Isaac and Ramesh Kulkarni. Super resolution techniques for medical image processing. In *ICTSD*, 2015. 1
- [16] Yuhang Li, Ruihao Gong, Xu Tan, Yang Yang, Peng Hu, Qi Zhang, Fengwei Yu, Wei Wang, and Shi Gu. Breq: Pushing the limit of post-training quantization by block reconstruction. In *ICLR*, 2021. 1
- [17] Zhikai Li, Junrui Xiao, Lianwei Yang, and Qingyi Gu. Repqv: Scale reparameterization for post-training quantization of vision transformers. In *ICCV*, 2023. 2, 6, 7
- [18] Jingyun Liang, Jiezhong Cao, Guolei Sun, Kai Zhang, Luc Van Gool, and Radu Timofte. Swinir: Image restoration using swin transformer. In *ICCVW*, 2021. 2, 5, 6, 7
- [19] Bee Lim, Sanghyun Son, Heewon Kim, Seungjun Nah, and Kyoung Mu Lee. Enhanced deep residual networks for single image super-resolution. In *CVPRW*, 2017. 2, 5
- [20] Kai Liu, Haotong Qin, Yong Guo, Xin Yuan, Linghe Kong, Guihai Chen, and Yulun Zhang. 2dquant: Low-bit post-training quantization for image super-resolution. *NeurIPS*, 2024. 2, 3, 5, 6, 7
- [21] Yijiang Liu, Huanrui Yang, Zhen Dong, Kurt Keutzer, Li Du, and Shanghang Zhang. Noisyquant: Noisy bias-enhanced post-training activation quantization for vision transformers. In *CVPR*, 2023. 2, 6, 7
- [22] David Martin, Charless Fowlkes, Doron Tal, and Jitendra Malik. A database of human segmented natural images and its application to evaluating segmentation algorithms and measuring ecological statistics. In *ICCV*, 2001. 5
- [23] Yusuke Matsui, Kota Ito, Yuji Aramaki, Azuma Fujimoto, Toru Ogawa, Toshihiko Yamasaki, and Kiyoharu Aizawa. Sketch-based manga retrieval using manga109 dataset. *Multi-media Tools and Applications*, 2017. 5
- [24] Adam Paszke, Sam Gross, Francisco Massa, Adam Lerer, James Bradbury, Gregory Chanan, Trevor Killeen, Zeming Lin, Natalia Gimelshein, Luca Antiga, et al. Pytorch: An imperative style, high-performance deep learning library. *NeurIPS*, 2019. 5
- [25] Pejman Rasti, Tönis Uiboupin, Sergio Escalera, and Gholamreza Anbarjafari. Convolutional neural network super resolution for face recognition in surveillance monitoring. In *AMDO*, 2016. 1
- [26] Radu Timofte, Eirikur Agustsson, Luc Van Gool, Ming-Hsuan Yang, Lei Zhang, Bee Lim, Sanghyun Son, Heewon Kim, Seungjun Nah, Kyoung Mu Lee, et al. Ntire 2017 challenge on single image super-resolution: Methods and results. In *CVPRW*, 2017. 5
- [27] Zhijun Tu, Jie Hu, Hanting Chen, and Yunhe Wang. Toward accurate post-training quantization for image super resolution. In *CVPR*, 2023. 6, 7
- [28] A.M. Turing. Rounding-off errors in matrix processes. *The Quarterly Journal of Mechanics and Applied Mathematics*, 1948. 2
- [29] J. von Neumann and H.H. Goldstine. Numerical inverting matrices of high order. *Bulletin of the American Mathematical Society*, 1947. 2
- [30] Zhou Wang, Alan C Bovik, Hamid R Sheikh, and Eero P Simoncelli. Image quality assessment: from error visibility to structural similarity. *TIP*, 2004. 5
- [31] Rongyuan Wu, Lingchen Sun, Zhiyuan Ma, and Lei Zhang. One-step effective diffusion network for real-world image super-resolution. *arXiv*, 2024. 1
- [32] Lechao Xiao, Yasaman Bahri, Jascha Sohl-Dickstein, Samuel S. Schoenholz, and Jeffrey Pennington. Dynamical isometry and a mean field theory of cnns: How to train 10,000-layer vanilla convolutional neural networks. *ICML*, 2018. 2

- [33] Zhihang Yuan, Chenhao Xue, Yiqi Chen, Qiang Wu, and Guangyu Sun. Ptq4vit: Post-training quantization framework for vision transformers. *ECCV, 2022*. [2](#), [6](#), [7](#)
- [34] Roman Zeyde, Michael Elad, and Matan Protter. On single image scale-up using sparse-representations. In *Proc. 7th Int. Conf. Curves Surf.*, 2010. [5](#)
- [35] Aozhong Zhang, Naigang Wang, Yanxia Deng, Xin Li, Zi Yang, and Penghang Yin. Magr: Weight magnitude reduction for enhancing post-training quantization. *NeurIPS, 2024*. [2](#)
- [36] Liangpei Zhang, Hongyan Zhang, Huanfeng Shen, and Pingxiang Li. A super-resolution reconstruction algorithm for surveillance images. *Elsevier Signal Processing*, 2010. [1](#)
- [37] Yulun Zhang, Kunpeng Li, Kai Li, Lichen Wang, Bineng Zhong, and Yun Fu. Image super-resolution using very deep residual channel attention networks. In *ECCV, 2018*. [2](#)
- [38] Yulun Zhang, Yapeng Tian, Yu Kong, Bineng Zhong, and Yun Fu. Residual dense network for image super-resolution. In *CVPR, 2018*. [2](#)